



Originally published as:

Karplus, M. S., Klemperer, S. L., Lawrence, J. F., Zhao, W., Mechie, J., Tilmann, F., Sandvol, E., Ni, J. (2013): Ambient-noise tomography of north Tibet limits geological terrane signature to upper-middle crust. - *Geophysical Research Letters*, 40, 5, 808-813

DOI: [10.1002/grl.50202](https://doi.org/10.1002/grl.50202)

Ambient-noise tomography of north Tibet limits geological terrane signature to upper-middle crust

M. S. Karplus,^{1,2} S. L. Klemperer,¹ J. F. Lawrence,¹ W. Zhao,³ J. Mechie,⁴ F. Tilmann,⁴ E. Sandvol,⁵ and J. Ni⁶

Received 20 November 2012; revised 23 January 2013; accepted 27 January 2013; published 6 March 2013.

[1] We use ambient-noise tomography to map regional differences in crustal Rayleigh-wave group velocities with periods of 8–40 s across north Tibet using the International Deep Profiling of Tibet and the Himalaya phase IV arrays (132 stations, deployed for 10–24 months). For periods of 8–24 s (sensitive to midcrustal depths of ~5–30 km), we observe striking velocity changes across the Bangong-Nujiang and Jinsha suture zones as well as the Kunlun-Qaidam boundary. From south to north, we see higher velocities beneath the Lhasa terrane, lower velocities beneath the Qiangtang, higher velocities in the Songpan-Ganzi and Kunlun terranes, and the lowest velocities beneath the Qaidam Basin. Maps at periods of 34 and 40 s (sensitive to the middle and lower crust at depths of ~30–60 km) do not show evidence of changes across those boundaries. Any differences between the Tibetan terrane lower crusts that were present at accretion have been erased or displaced by Cenozoic processes and replaced almost ubiquitously by uniformly low velocities. **Citation:** Karplus, M. S., S. L. Klemperer, J. F. Lawrence, W. Zhao, J. Mechie, F. Tilmann, E. Sandvol, and J. Ni (2013), Ambient-noise tomography of north Tibet limits geological terrane signature to upper-middle crust, *Geophys. Res. Lett.*, 40, 808–813, doi:10.1002/grl.50202.

1. Introduction

[2] Since the pioneering deployment of long-period seismographs within Tibet in 1982 [Jobert *et al.*, 1985], numerous studies of surface-wave dispersion have been performed within Tibet using regional and teleseismic earthquakes [e.g., Huang *et al.*, 2003; Levshin *et al.*, 1994; Rapine *et al.*, 2003; Shapiro *et al.*, 2004] and ambient noise [e.g., Guo *et al.*, 2009; Li *et al.*, 2009; Yang *et al.*, 2010; Yao *et al.*, 2008]. However, the majority of regional studies reporting high-resolution crustal models are in southeast [e.g., Yao *et al.*,

2008] and southern Tibet [e.g., Guo *et al.*, 2009]. In this study, we use new data collected from stations in north Tibet deployed by project INDEPTH (International Deep Profiling of Tibet and the Himalaya), phase IV, to create a high-resolution crustal Rayleigh-wave model.

[3] In southern Tibet, researchers observe a low-velocity zone from surface waves in the middle crust [e.g., Caldwell *et al.*, 2009; Rapine *et al.*, 2003] and suggest that it supports the hypothesis of fluids in the middle crust first imaged using INDEPTH II active-source seismic data [Nelson *et al.*, 1996] and perhaps also supports the crustal-flow models proposed by Royden *et al.* [1997] and refined by Beaumont *et al.* [2004]. These crustal-flow models propose that the middle and/or lower crust is decoupled from the upper crust and upper mantle, allowing the middle-lower crust to flow outward from central Tibet, releasing gravitational potential energy of the high plateau and continued compression from the India-Asia collision [Klemperer, 2006]. However, recent studies suggest that low-velocity zones as well as electrically conductive zones in the middle and lower crust beneath south and southeastern Tibet may be discontinuous, with significant lateral variations and complex structure [Hetényi *et al.*, 2011; Yang *et al.*, 2012; Yao *et al.*, 2010].

[4] In north Tibet, recent wide-angle reflection and refraction results from INDEPTH IV [Karplus *et al.*, 2011] show that middle- and lower-crustal *P* wave velocities beneath the Songpan-Ganzi terrane and Kunlun Mountains are as low as those in southern Tibet, indicating the possibility of partial melt or other fluids within the crust and thus the possibility for flow. Reflector geometries were interpreted to indicate injection of Kunlun Mountains lower crust beneath Qaidam crust at or near the Moho [Karplus *et al.*, 2011]. Magnetotelluric data have been interpreted as showing north-directed midcrustal melt penetration across the north Kunlun fault [Le Pape *et al.*, 2012].

[5] We use ambient noise on continuous seismic records from north Tibet to construct empirical Green's functions (EGFs) and constrain Rayleigh-wave group velocities for periods of 8–40 s. Our model is well-resolved and sensitive to structure from ~5–60 km in the Lhasa, Qiangtang, Songpan-Ganzi (SG), Kunlun Mountains, and Qaidam terranes from approximately 91°E to 99°E and 31°N to 37°N.

2. Data and Methods

[6] Our data sources are vertical-component continuous recordings from the collaborative Chinese, U.S., German, and U.K. INDEPTH IV linear profiles and areal array, grouped according to the times they were deployed. Station group A (78 stations) was deployed nominally from June 2007 to September 2008. Station group B (24 stations) was

All Supporting Information may be found in the online version of this article.

¹Department of Geophysics, Stanford University, Stanford, California, USA.

²Now at School of Ocean and Earth Science, University of Southampton, Southampton, UK, USA.

³Chinese Academy of Geological Sciences, Beijing, China.

⁴Deutsches GeoForschungsZentrum – GFZ, Potsdam, Germany.

⁵Department of Geological Sciences, University of Missouri – Columbia, Columbia, Missouri, USA.

⁶Department of Physics, New Mexico State University, Las Cruces, New Mexico, USA.

Corresponding author: M. S. Karplus, School of Ocean and Earth Science, University of Southampton, Waterfront Campus, European Way, Southampton, UK SO14 3ZH. (M.S.Karplus@soton.ac.uk)

©2013. American Geophysical Union. All Rights Reserved.
1944-8007/13/10.1002/grl.50202

deployed from August 2008 to June 2009. Group C (30 stations) was deployed for the entire time period from June 2007 to June 2009 (Figure 1). Stations with < 10 days of recorded data are not used. Previous studies have used portions of these data for ambient noise studies [Yang *et al.*, 2010, 2012], but we add stations from dense, 1-D profiles crossing the Jinsha and Kunlun sutures thereby adding greater redundancy in north Tibet. Station pairs with interstation distances $\lesssim 30$ km do not produce reliable ambient noise results, even for our shortest periods of 8 s, due to scattering. However, the stations of the 1-D profiles paired with other stations of the regional array $\gtrsim 30$ km away give many two-station paths crossing the area around the 1-D profiles. We only use the vertical component noise, so that the cross-correlations contain only Rayleigh-wave signals [Bensen *et al.*, 2007].

[7] In the time domain, the cross-correlation of whitened ambient seismic noise at two stations yields a waveform resembling the EGF between them [Sanchez-Sesma and Campillo, 2006]. In this study, we obtain Rayleigh-wave dispersion measurements from interstation EGFs generated by the cross-correlation of seismic ambient noise using

well-established methods [Bensen *et al.*, 2007; Prieto *et al.*, 2009] (Supporting Information).

[8] Briefly, we obtain a group-velocity dispersion curve corresponding to each station pair using the multiple-filter technique [Dziewonski *et al.*, 1969] (Figure S1b–S1c). At periods shorter than 6 s the ambient field amplitude is sufficiently small that coherency does not persist for ≥ 50 km. Robust dispersion measurements can typically only be made up to a period equal to the interstation spacing (in km) divided by 12 [Bensen *et al.*, 2007]. We did not have a sufficient number of station pairs with interstation spacing > 500 km to measure dispersion at periods > 40 s.

[9] We then use an iterative conjugate-gradient least-squares inversion method [Paige and Saunders, 1982] to derive velocities for a block dispersion model with $0.1^\circ \times 0.1^\circ$ lateral block size, and 2 s increments of group velocity from 6 to 40 s. We perform checkerboard resolution tests to examine velocity recovery for different period slices (Figure 2) and report the velocity maps for those slices (Figure 3). We display this model as velocity vs. period curves for individual surface locations within the model (Figure 4).

3. Group-Velocity Results

3.1. Group-Velocity Maps

[10] Rayleigh-wave group-velocity maps at periods of 8–40 s are plotted in Figure 3. The approximate depths sampled by waves of various periods are shown in Figure S5 and noted in the text below. Decreased velocity with increased period need not correspond to an actual decrease of velocity with increasing depth [e.g., Shapiro *et al.*, 2004]. However, group-velocity variations with period approximate average shear velocities for different depth intervals of the crust but also strongly depend on velocity gradients within the depth range of sensitivity [Villaseñor *et al.*, 2007].

[11] We observe striking velocity contrasts from 8 to 24 s (down to ~ 30 km depth) across many of the major regional terrane boundaries and faults. At periods less than 24 s, the Bangong-Nujiang Suture appears to separate higher Lhasa terrane velocities from lower Qiangtang velocities, but the velocities become similar for longer periods. This suggests a faster Lhasa upper crust compared to the Qiangtang, confirming and extending into new geographic areas similar observations from INDEPTH III *P* wave modeling at 89°E [Haines *et al.*, 2003]. Rapine *et al.* [2003] observed the opposite trend in surface-wave group velocities (slower Lhasa upper crust compared to the Qiangtang) using earthquakes, albeit averaging along E-W paths over a larger area from $\sim 80^\circ\text{E}$ – 90°E . They also observed lower group velocities at almost all periods, perhaps suggesting lateral heterogeneity or anisotropy.

[12] The Qiangtang terrane has several localized, shallow low-velocity anomalies (~ 0.1 – 0.15 km/s below average for the period slice). From 8–24 s, the Jinsha suture separates lower-velocity Qiangtang terrane from higher-velocity Songpan-Ganzi, but velocities at longer periods, 34–40 s (depths ~ 30 – 60 km), are similar across the Jinsha suture.

[13] A strong high-velocity anomaly of > 0.15 km/s above the period average is observed beneath the SG terrane between $\sim 93^\circ\text{E}$ – 96°E , at periods < 24 s. There appears to be a narrower N-S-oriented high-velocity anomaly beneath the SG at 34–40 s. This anomaly may represent a subterranean within the SG, although lack of basement outcrop in this

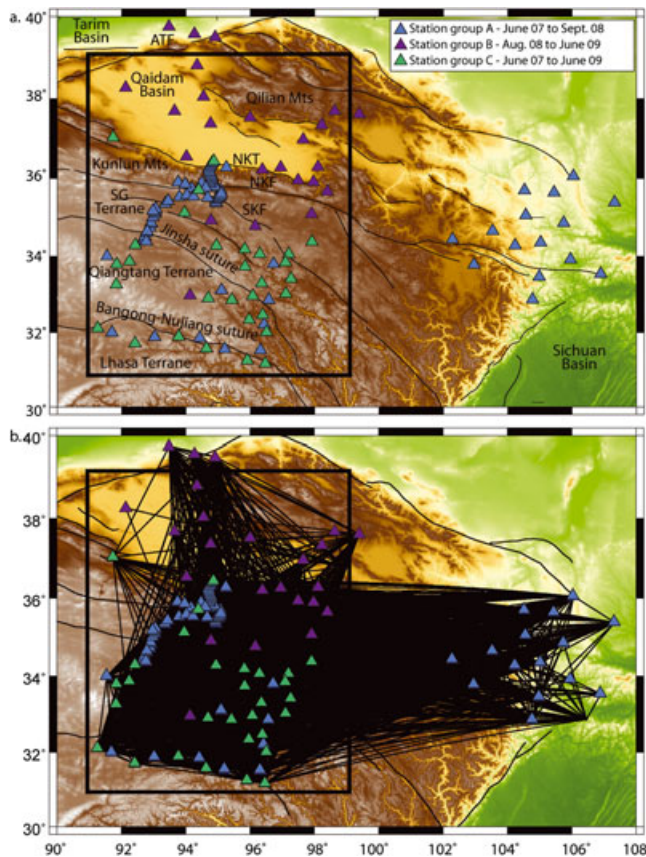


Figure 1. (a) Map showing stations for the INDEPTH IV arrays, colored by deployment dates. Stations recording fewer than 10 days of data are omitted. Rectangle encloses the study area shown in Figures 2 and 3. (b) Two-station path coverage actually used in our ambient-noise tomography. Not all stations successfully recorded data during the full deployment of the array. ATF: Alтын Tagh fault; NKT: North Kunlun thrust system; NKF: North Kunlun fault; SKF: South Kunlun fault; SG: Songpan Ganzi.

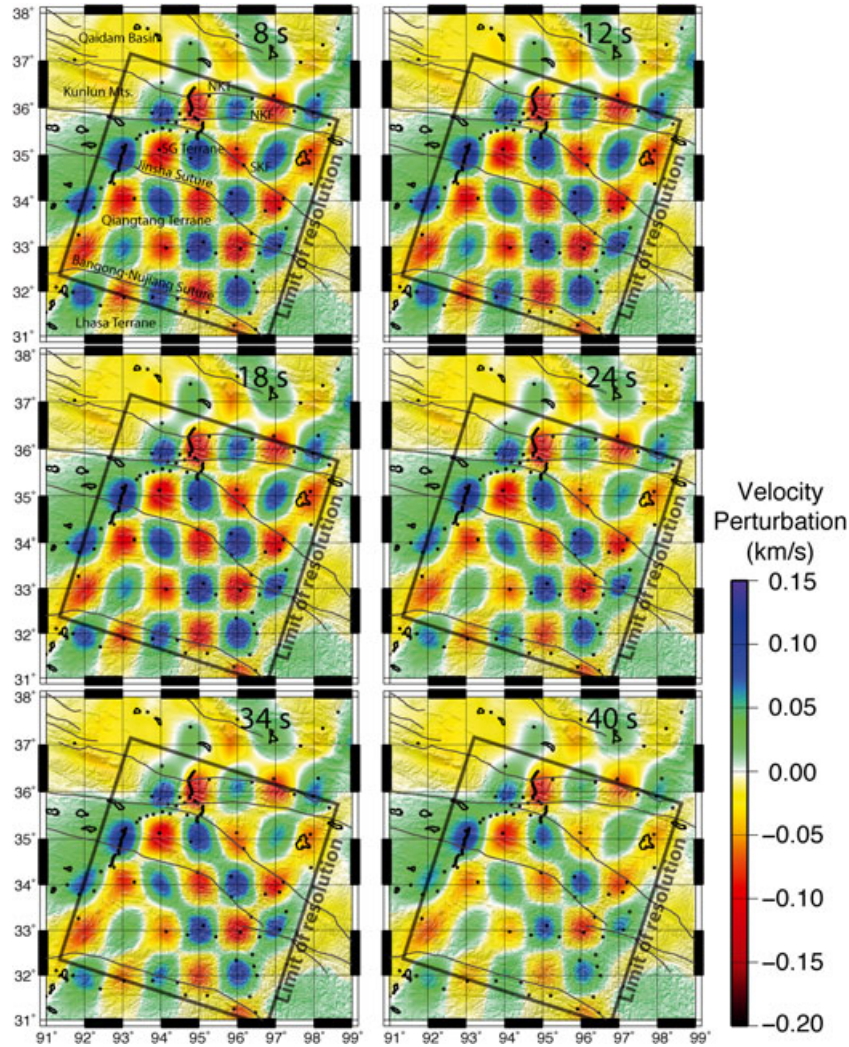


Figure 2. Results of a checkerboard test with columnar $1^\circ \times 1^\circ$ lateral anomalies. Black dots indicate stations.

region of Tibet limits our geologic interpretation of this anomaly.

[14] High-velocity anomalies of 0.05–0.10 km/s are seen in the Kunlun Mountains between the north Kunlun thrust (NKT) and the north Kunlun fault for periods < 24 s. These high velocities are likely due to intrusives of the Kunlun batholith.

[15] The slow velocity anomaly of up to ~ 0.15 km/s associated with the Qaidam Basin is clearly observed for periods < 18 s and less strongly, to 24 s, consistent with known thicknesses of Qaidam sedimentary rocks up to 15 km thick in the center of the basin [Yin *et al.*, 2007], and relatively high shear-wave velocities beneath Qaidam compared to the Songpan-Ganzi between ~ 22 –30 km depth [e.g., Ceylan *et al.*, 2012; Mechie *et al.*, 2012].

[16] Our group-velocity maps are broadly consistent with the phase-velocity maps of Yang *et al.* [2012] at 10 s. At 40 s, the maps are also similar, except that we record a strong fast anomaly beneath the Songpan-Ganzi at 93°E – 95°E and 34.5°N – 35.5°N , near our densest station coverage.

[17] Our velocity anomalies are also broadly consistent with the phase-velocity maps produced by Ceylan *et al.* [2012] using two-plane-wave tomography for waves with periods from 24 to 40 s. The one large difference between

the results of our paper and Yang *et al.* [2012] compared to Ceylan *et al.* [2012] is that Ceylan *et al.* [2012] showed significantly higher velocities (up to ~ 0.2 km/s higher) beneath the Qaidam Basin from 24 to 40 s compared to the Kunlun Mountains and Songpan-Ganzi to the south. This result is puzzling given that all three papers used the same INDEPTH IV regional stations across the Qaidam Basin, but may be an artifact of the different methods combined with generally poor resolution in the Qaidam Basin. Ceylan *et al.* [2012] also did not image the strong fast anomaly that we find, seemingly well-resolved within our densest station coverage, beneath the Songpan-Ganzi at 93°E – 95°E and 34.5°N – 35.5°N .

3.2. Group-Velocity Dispersion Curves

[18] We extract Rayleigh-wave group-velocity dispersion curves from our velocity model every 0.5° latitude along a N-S profile along 95°E (Figure 4), along which we have good model recovery at all points from 32°N to 36°N (Figure 2). Our longest period Rayleigh waves, 40 s, are most sensitive to depths of 30–40 km, insufficient to sense the mantle in Tibet where the Moho is ~ 70 km deep south of the NKT and ~ 50 km deep beneath the Qaidam Basin [Karplus *et al.*, 2011].

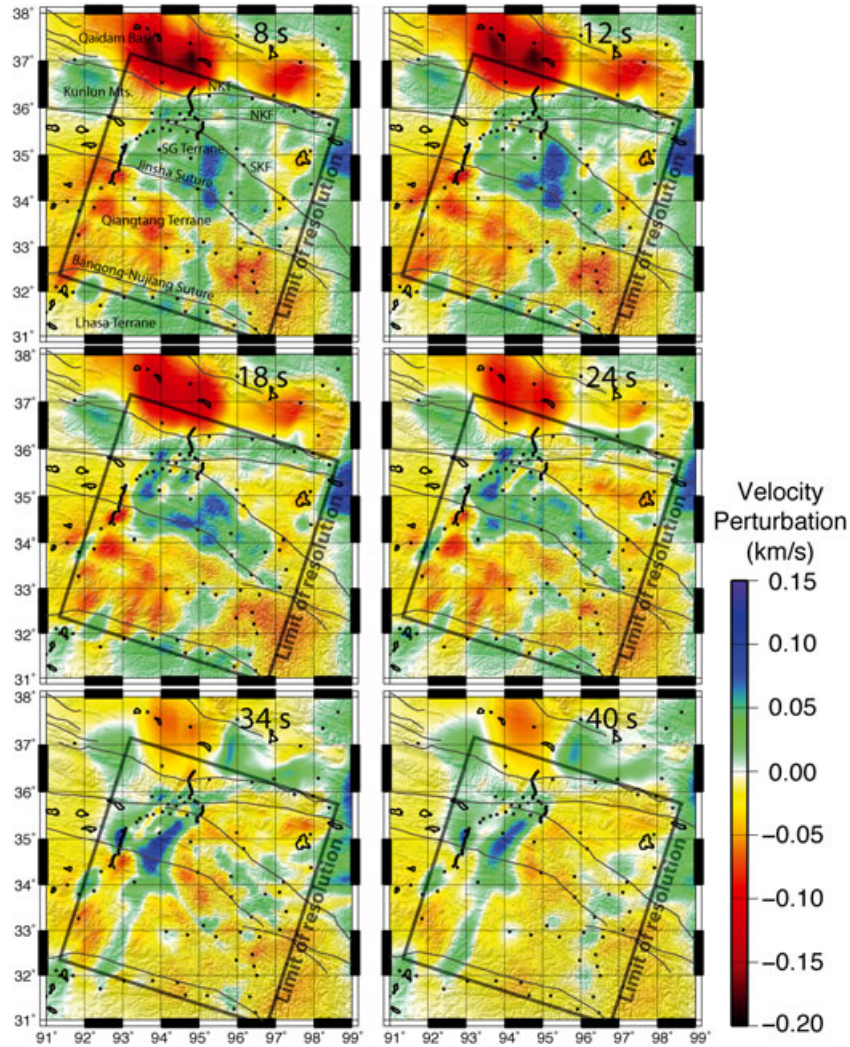


Figure 3. Rayleigh wave group velocity maps showing velocity perturbations from the average velocity for each slice. Average velocities for each period slice are: 8 s – 2.99 km/s, 12 s – 3.04 km/s, 18 s – 3.02 km/s, 24 s – 2.99 km/s, 34 s – 3.09 km/s, 40 s – 3.16 km/s. NKT: North Kunlun thrust system; NKF: North Kunlun fault; SKF: South Kunlun fault; SG: Songpan Ganzi; JS – Jinsha suture; BNS – Bangong-Nujiang suture.

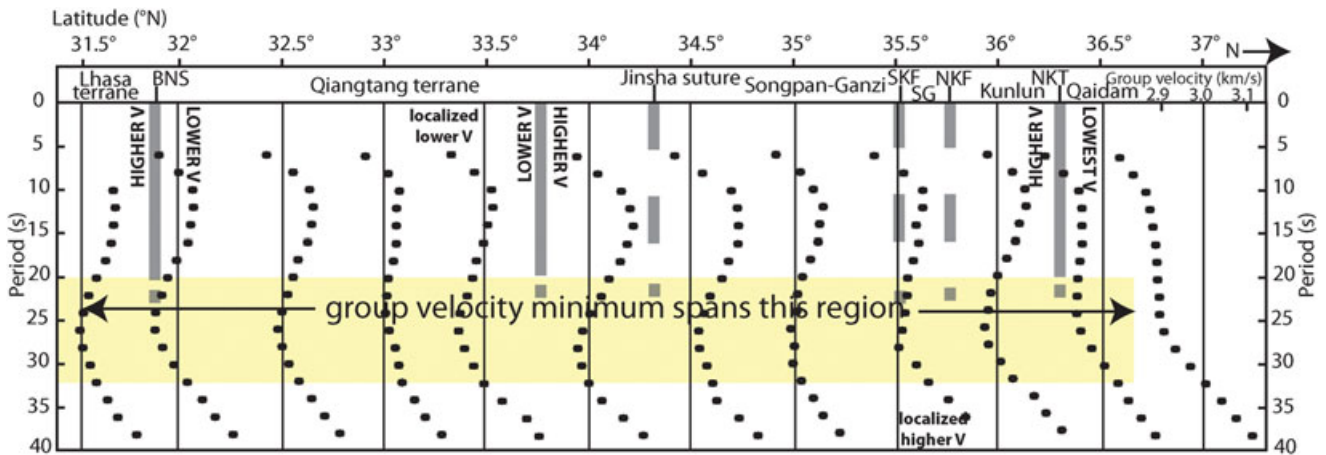


Figure 4. Group-velocity dispersion curves extracted from the tomographic model every 0.5° latitude from 31.5°N–37°N for a N-S profile along 95°E. Yellow shading; marks group velocity minimum; SKF – South Kunlun Fault; NKF – North Kunlun Fault; NKT – North Kunlun Thrusts; BNS – Bangong-Nujiang Suture; SG – Songpan-Ganzi. Vertical black lines are fiducial lines indicating a group velocity of 3 km/s. Solid gray lines indicate locations of significant changes in velocity structure.

[19] The most striking feature of this dispersion curve profile is that almost all curves show group velocities decreasing with period between ~15–25 s (Figure 4). Group velocities decrease by as much as ~0.1 km/s at 34°N (just south of Jinsha suture) and 36°N (just north of NKT). In contrast, dispersion curves are flat in the same period range at 33°N (central Qiangtang terrane) and 37°N (Qaidam Basin).

[20] The decrease in group velocity at periods > 20 s is most evident where we find the highest group velocities at ~10 s period (upper-middle crust) of 3.11 km/s (~0.04 km/s higher than surrounding areas of the same period/depth) at 34.5°N (south of the south Kunlun fault in the Songpan-Ganzi terrane). Conversely, there is no midcrustal decrease in group velocity north of 36.5°N, within the Qaidam Basin, where we find the lowest, short-period (~10 s) velocity at ~2.8 km/s, presumably due to the sedimentary rocks in the basin known to reach depths > 15 km [e.g., Yin *et al.*, 2007].

[21] Down to ~30 km (sampled by periods of \lesssim 24 s), changes in upper- to middle-crustal velocities occur across the suture zones. The velocity change from the Qiangtang to the SG terrane is 10–50 km south of the suture perhaps corresponding to the geologically inferred gentle southward dip [Kapp *et al.*, 2003]; the other velocity changes are more closely aligned with surface faults implying more vertical structures. The sutures may have been erased in the lower crust, possibly by crustal flow, because the lateral velocity differences are much smaller at periods corresponding to the middle-lower crust than at periods representative of the upper crust.

4. Discussion and Implications for Geodynamics

[22] Our robust Rayleigh-wave group-velocity model for waves from 8 to 40 s for the north Tibetan Plateau was derived using ambient-noise tomography with stations of the INDEPTH IV linear and regional arrays. Our model adds new detail to our structural understanding of north Tibet while confirming known broad-scale features seen in previous studies of ambient noise and earthquake surface-wave tomography. The combination of the INDEPTH IV linear profiles and areal array gives us the densest ray-path coverage yet available across the north Qiangtang, Songpan-Ganzi, Kunlun, and Qaidam regions between 92°E–98°E.

[23] Above ~30 km depth, the Rayleigh-wave group-velocity contrasts across the Bangong-Nujiang suture (8–24 s), the Jinsha suture (8–24 s), the south Kunlun fault (18–24 s), the north Kunlun fault (18–24 s), and the north Kunlun thrust (8–24 s) likely mark terrane or block boundaries. If this is the case, the upper ~30 km of the crust may be deforming as coherent blocks, and any decoupling layer must be deeper than ~30 km. The major sutures are no longer evident in velocity maps at 34 and 40 s (below ~30 km), consistent with lower-crustal flow having erased or displaced velocity contrasts in the lower crust and suggestive that the middle-to-lower crust may be decoupled from the upper crust and deforming continuously [cf. Yang *et al.*, 2012]. This is consistent with the observation that seismicity across north Tibet is restricted to the upper 20–30 km of the crust [Wei *et al.*, 2010] and with the view from controlled-source seismic data that the north and south Kunlun faults do not extend below 20–30 km [Karplus *et al.*, 2011], and the

Bangong-Nujiang suture does not extend near-vertically below about 30 km [Haines *et al.*, 2003].

[24] Yang *et al.* [2012] observed a low shear-velocity zone at ~30 km (sampled by waves with period 24 s) across most of the Tibetan Plateau marked by a velocity minimum in the 1-D vertical velocity-depth model. The low velocities are most marked near the boundaries of the Tibetan Plateau [Yang *et al.*, 2012]. We also see a group-velocity minimum at ~24 s (sampling depths of ~30 km). In our study area, the most marked velocity minimum is seen near the Kunlun-Qaidam boundary.

[25] Previous studies have explored whether the presence of a low-velocity zone indicates midcrustal partial melting perhaps initiated by the presence of aqueous fluids [Caldwell *et al.*, 2009; Yang *et al.*, 2012]. Widespread fluids have been inferred from 25 to 50 km depth at 32.5°N–35.5°N, 92°E–94°E [Unsworth *et al.*, 2004]. Hence, our velocity minimum, which may correspond to the low-velocity zones from previous studies, and that underlies a large area of north Tibet (~32°N–36°N), may indicate a region of partial melt or of aligned anisotropic minerals [Yang *et al.*, 2012] and almost certainly indicates an area of significant crustal weakness [e.g., Klempner, 2006] and substantial middle-to-lower crustal deformation that may continue today as a distributed shear zone [Yang *et al.*, 2012]. The northern limit of the low group velocities is broadly consistent with the location where Karplus *et al.* [2011] suggested northward injection of the Kunlun Mountains crust into the Qaidam Basin.

[26] **Acknowledgments.** INDEPTH activities are funded by NSF grants (EAR-CD-0409939, EAR-0634904, EAR-0409589), Deutsche Forschungsgemeinschaft, GFZ Potsdam, and CGS-1212010511809 in China. An NSF graduate fellowship supported M. Karplus. We thank the INDEPTH field teams. Instruments were provided by IRIS-PASSCAL, NERC-SEISUK, and GFZ-GIPP. The seismic data is archived in the IRIS Data Management Center (networks XO, X4, and Z1) and the GFZ GEOFON database (network XO). We thank N. Harmon for assistance with the group-velocity sensitivity calculation. We thank N. Rawlinson and an anonymous reviewer for suggestions to improve the manuscript.

References

- Beaumont, C., R. A. Jamieson, M. H. Nguyen, and S. Medvedev (2004), Crustal channel flows: 1. Numerical models with applications to the tectonics of the Himalayan-Tibetan orogen, *J. Geophys. Res.*, *109*, doi:10.1029/2003JB002809.
- Bensen, G. D., M. H. Ritzwoller, M. P. Barmin, A. I. Levshin, F. Lin, M. P. Moschetti, N. M. Shapiro, and Y. Yang (2007), Processing seismic ambient noise data to obtain reliable broad-band surface wave dispersion measurements, *Geophys. J. Int.*, *169*, 1239–1260.
- Caldwell, W. B., S. L. Klempner, S. S. Rai, and J. F. Lawrence (2009), Partial melt in the upper-middle crust of the northwest Himalayas revealed by Rayleigh wave dispersion, *Tectonophysics*, *477*, 58–65, doi:10.1016/j.tecto.2009.01.013.
- Ceylan, S., J. Ni, Y. J. Chen, Q. Zhang, F. Tilmann, and E. Sandvol (2012), Fragmented Indian plate and vertically coherent deformation beneath eastern Tibet, *J. Geophys. Res.*, *117*, doi:10.1029/2012JB009210.
- Dziewonski, A., S. Bloch, and M. Landisman (1969), A technique for the analysis of transient seismic signals, *Bull. Seis. Soc. Am.*, *59*(1), 427–444.
- Guo, Z., X. Gao, H. Yao, J. Li, and W. Wang (2009), Midcrustal low-velocity layer beneath the central Himalaya and southern Tibet revealed by ambient noise array tomography, *Geochem. Geophys. Geosys.*, *10*(5), doi:10.1029/2009GC002458.
- Haines, S., S. L. Klempner, L. D. Brown, J. Guo, J. Mechie, R. Meissner, A. Ross, and W. Zhao (2003), INDEPTH III seismic data: From surface observations to deep crustal processes in Tibet, *Tectonics*, *22*, doi:10.1029/2001TC001305.
- Hetényi, G., J. Vergne, L. Bollinger, and R. Cattin (2011), Discontinuous low-velocity zones in southern Tibet question the viability of the channel flow model, *Geol. Soc. Lond. Spec. Publ.*, *353*, 99–108.

- Huang, Z. X., W. Su, Y. J. Peng, Y. J. Zheng, and H. Y. Li (2003), Rayleigh wave tomography of China and adjacent regions, *J. Geophys. Res.*, *108*(B2), 2073, doi:10.1029/2001JB001696.
- Jobert, N., B. Jourmet, G. Jobert, A. Hirn, and S. K. Zhong (1985), Deep structure of southern Tibet inferred from the dispersion of Rayleigh waves through a long-period seismic network, *Nature*, *313*, 386–388, doi:10.1038/313386a0.
- Kapp, P., A. Yin, C. E. Manning, T. M. Harrison, M. H. Taylor, and L. Ding (2003), Tectonic evolution of the early Mesozoic blueschist-bearing Qiangtang metamorphic belt, central Tibet, *Tectonics*, *22*(4), doi:10.1029/2002TC001383.
- Karplus, M. S., W. Zhao, S. L. Klemperer, Z. Wu, J. Mechie, D. Shi, L. D. Brown, and C. Chen (2011), Injection of Tibetan crust beneath the south Qaidam Basin: Evidence from INDEPTH IV wide angle seismic data, *J. Geophys. Res.*, *116*, doi:10.1029/2010JB007911.
- Klemperer, S. (2006), Crustal flow in Tibet: geophysical evidence for the physical state of Tibetan lithosphere, and inferred patterns of active flow, in *Channel flow, ductile extrusion and exhumation in continental collision zones*, *Geol. Soc. Spec. Pub.*, *268*, 39–70.
- Le Pape, F., A. G. Jones, J. Vozar, and W. Wenbo (2012), Penetration of crustal melt beyond the Kunlun Fault into northern Tibet, *Nat. Geosci.*, *5*(5), 1–6, doi:10.1038/ngeo1449.
- Levshin, A. I., M. H. Ritzwoller, and L. I. Ratnikova (1994), The nature and cause of polarization anomalies of surface waves crossing northern and central Eurasia, *Geophys. J. Int.*, *117*, 577–590.
- Li, H., W. Su, C.-Y. Wang, and Z. Huang (2009), Ambient noise Rayleigh wave tomography in western Sichuan and eastern Tibet, *Earth Planet. Sci. Lett.*, *282*, 201–211.
- Mechie, J., et al. (2012), Crustal shear (S) velocity and Poisson's ratio structure along the INDEPTH IV profile in northeast Tibet as derived from wide-angle seismic data. *Geophys. J. Int.*, doi: 10.1111/j.1365-246X.2012.05616.x.
- Nelson, K. D., et al. (1996), Partially molten middle crust beneath southern Tibet: synthesis of project INDEPTH results, *Science*, *274*(5293), 1684–1688, doi:10.1126/science.274.5293.1684.
- Paige, C. C., and M. A. Saunders (1982), LSQR: an algorithm for sparse linear equations and sparse least squares, *Assoc. Comput. Mach. Trans. Math. Software*, *8*(1), 43–71.
- Prieto, G. A., J. F. Lawrence, and G. C. Beroza (2009), Anelastic Earth structure from the coherency of the ambient seismic field, *J. Geophys. Res.*, *114*, B07303, doi:10.1029/2008JB006067.
- Rapine, R., F. Tilmann, M. West, J. Ni, and A. Rogers (2003), Crustal structure of northern and southern Tibet from surface wave dispersion analysis, *J. Geophys. Res.*, *108*(B2), 2120, doi:10.1029/2001JB000445.
- Royden, L. H., B. C. Burchfiel, R. W. King, E. Wang, Z. L. Chen, F. Shen, and Y. P. Liu (1997), Surface deformation and lower crustal flow in eastern Tibet, *Science*, *276*, 788–790, doi:10.1126/science.276.5313.788.
- Sanchez-Sesma, F. J., and M. Campillo (2006), Retrieval of the Green's function from cross correlation: The canonical elastic problem, *Bull. Seis. Soc. Am.*, *96*(3), 1182–1191, doi:10.1785/0120050181.
- Shapiro, N. M., M. H. Ritzwoller, P. Molnar, and V. Levin (2004), Thinning and flow of Tibetan crust constrained by seismic anisotropy, *Science*, *305*, 233–236, doi:10.1126/science.1098276.
- Unsworth, M., W. Wei, A. G. Jones, S. Li, P. Bedrosian, J. Booker, S. Jin, M. Deng, and H. Tan (2004), Crustal and upper mantle structure of northern Tibet imaged with magnetotelluric data, *J. Geophys. Res.*, *109*, doi:10.1029/2002JB002305.
- Villaseñor, A., Y. Yang, M. Ritzwoller, and J. Gallart (2007), Ambient noise surface wave tomography of the Iberian Peninsula: Implications for shallow seismic structure, *Geophys. Res. Lett.*, *34*, L11304, doi:10.1029/2007GL030164.
- Wei, S., et al. (2010), Regional earthquakes in northern Tibetan Plateau: Implications for lithospheric strength in Tibet, *Geophys. Res. Lett.*, *37*, L19307, doi:10.1029/2010GL044800.
- Yang, Y., M. H. Ritzwoller, Y. Zheng, W. Shen, A. L. Levshin, and Z. Xie (2012), A synoptic view of the distribution and connectivity of the mid-crustal low velocity zone beneath Tibet, *J. Geophys. Res.*, *117*(B4), 1–20, doi:10.1029/2011JB008810.
- Yang, Y., et al. (2010), Rayleigh wave phase velocity maps of Tibet and the surrounding regions from ambient seismic noise tomography, *Geochem. Geophys. Geosyst.*, *11*(8), doi:10.1029/2010GC003119.
- Yao, H., C. Beghein, and R. D. van der Hilst (2008), Surface wave array tomography in SE Tibet from ambient seismic noise and two-station analysis: II—Crustal and upper mantle structure, *Geophys. J. Int.*, *173*(1), 205–219, doi:10.1111/j.1365-246X.2007.03696.x.
- Yao, H., R. D. van der Hilst, and J.-P. Montagner (2010), Heterogeneity and anisotropy of the lithosphere of SE Tibet from surface wave array tomography, *J. Geophys. Res.*, *115*, B12307, doi:10.1029/2009JB007142.
- Yin, A., Y.-Q. Dang, M. Zhang, M. W. McRivette, W. P. Burgess, and X. Chen (2007), Cenozoic tectonic evolution of Qaidam basin and its surrounding regions (part 2): Wedge tectonics in southern Qaidam basin and the Eastern Kunlun Range, *GSA Special Paper 433*, 369–390, doi:10.1130/2007.2433(18).